Materials & Design 262 (2026) 115478

Contents lists available at ScienceDirect

Materials & Design

journal homepage: www.elsevier.com/locate/matdes

From billet to extruded band: Engineering texture and properties in AA6082 through die design and billet condition

Maria Nienaber [a,*], Fabian Esterl [b,**], Noomane Ben Khalifa [a,b], Jan Bohlen [a]

[a] Institute of Material and Process Design, Helmholtz-Zentrum Hereon, Geesthacht, Germany
[b] Institute for Production Technology and Systems, Leuphana Universität Lüneburg, Lüneburg, Germany

ARTICLE INFO

Keywords:
AA6082
Extrusion
Texture
Mechanical properties
Billet remainder
Initial material
Die design

ABSTRACT

This study investigates the influence of billet condition and die design on the microstructure, texture evolution, and mechanical properties of extruded AA6082 flat bands. Using cast and pre-extruded billets, profiles were produced with a conventional flat die and a modified die featuring a different press channel geometry, thereby altering local deformation conditions. Electron backscatter diffraction (EBSD) analyses were performed on both final profiles and billet remainders to trace texture development along the extrusion path. Pre-extruded billets showed enhanced recrystallization and finer, more homogeneous grain structures, while cast billets retained deformation textures and required higher strain accumulation to activate recrystallization nucleation mechanisms. The modified die promoted Goss texture formation and reduced peripheral coarse grain zones, resulting in improved ductility and reduced anisotropy. Finite element simulations confirmed smoother strain introduction in the modified die route, facilitating dynamic recrystallization. Mechanical testing revealed that the combination of pre-extruded billets and modified die yielded the most favorable properties, including high tensile strength and uniform elongation. These findings highlight the critical role of initial microstructure and strain path engineering in tailoring texture and mechanical performance in aluminum extrusion, offering practical guidance for optimizing lightweight structural components.

1. Introduction

Aluminum alloys of the 6xxx series, particularly AA6082, are widely employed in structural applications across the automotive, aerospace, and construction sectors due to their favorable balance of mechanical strength, corrosion resistance, and formability. As a heat-treatable alloy, AA6082 offers significant potential for property tailoring through thermomechanical processing, with hot extrusion being one of the most emphasized forming techniques.

The mechanical behavior of extruded aluminum products is governed not only by alloy composition and heat treatment but also by the evolution of microstructure and crystallographic texture during deformation, as well as the dominating types of dynamic recrystallization (DRX) mechanisms, such as continuous dynamic recrystallization (CDRX), discontinuous dynamic recrystallization (DDRX), and geometrical dynamic recrystallization (GDRX). Acting simultaneously with deformation, these mechanisms refine the grain structure and determine the developing texture [1–3]. This texture, in turn, influences anisotropy, yield strength, and ductility [4–6]. In face-centered cubic (FCC) metals such as aluminum, typical recrystallization textures include Cube {001} < 100 > and Goss {110} < 001>, while deformation textures such as Brass {110} < 112>, Copper {112} < 1–10>, and S {123} < 634 > often dominate in the early stages of strain accumulation [7–11]. It has been proposed by Samajdar et al. [12] that Cube-oriented grains exhibit preferential recovery during annealing, thereby retaining lower stored energy compared to other orientations. Concurrently, S-oriented grains, which are typically associated with deformation textures, undergo recrystallization and are transformed into Cube-oriented grains. This transformation is believed to occur either through nucleation of cube grains at the boundaries of S-oriented grains or via preferential growth mechanisms, ultimately contributing to the development of a strong cube texture in the recrystallized microstructure. According to findings by Hjelen et al. [13], Cube-oriented grains in aluminum tend to nucleate preferentially from transition bands located within the Copper or ND-rotated Copper texture components. In contrast, recrystallized grains exhibiting the Goss orientation primarily

* Corresponding author.
** Corresponding author.
E-mail addresses: maria.nienaber@hereon.de (M. Nienaber), fabian.esterl@leuphana.de (F. Esterl).

https://doi.org/10.1016/j.matdes.2026.115478
Received 3 September 2025; Received in revised form 18 December 2025; Accepted 9 January 2026
Available online 11 January 2026

originate from transition zones within the Brass component or from regions situated between the Brass and Goss deformation components. In a recent study by Sun et al. [2], the formation of cube texture in aluminum was attributed to the preferential acquisition of growth-driving forces via grain boundary migration mechanisms, specifically GDRX and DDRX. Chen et al. [14] emphasized that Goss-oriented grains can originate from recrystallization within Cube bands. In contrast to Cube orientation, which is mainly caused by primary recrystallization, secondary recrystallization, in which selective grain growth and nucleation in shear bands play a role, is usually responsible for the Goss component [15–17].

During extrusion, the formation and development of texture components depend on the state variables that trigger distinct deformation and recrystallization kinetics, which are present in the forming zone. Li et al. [18] have shown that the evolution of recrystallization textures in Al–Cu-based alloys is significantly influenced by extrusion parameters such as extrusion ratio, temperature, and speed. In particular, Cube and Goss orientations have been identified as soft texture components that primarily originate from recrystallized grains, while deformation textures, such as with Copper orientations, are associated with higher dislocation densities and originate from deformed grains. Besides these traditional extrusion parameters, the strain path can be influenced as a result of an altered die design [19–21], thereby changing the local deformation conditions [17,22–24]. Modified die designs, such as those incorporating pre-chambers or tailored press channels, have been shown to alter the strain distribution and promote more homogeneous recrystallization [21], thereby also mitigating peripheral coarse grain (PCG) formation [25,26].

While the literature clearly points towards the importance of the initial billet condition and the die geometry on the resulting microstructure and texture, their interaction during extrusion has not yet been systematically investigated. Particularly, the origin of recrystallization textures developing along the extrusion paths and their connection to specific deformation modes remains largely unknown. Therefore, this study aims to investigate the microstructure–texture–property relationships in extruded AA6082 flat bands by examining the combined effects of initial billet condition and die design. To explore the origin and progression of texture development, microstructural analysis via electron backscatter diffraction (EBSD) was performed not only on the final profiles but also on the billet remainder. Mechanical testing in multiple orientations provides insight into the anisotropic response of the material and its correlation with microstructure and texture features. The results contribute to a deeper understanding of texture development in aluminum (AA6082) extrusion, offering practical guidance for optimizing process parameters to achieve tailored mechanical properties in lightweight structural components.

2. Materials and Methods

In this study, extrusion trials were carried out using two distinct initial conditions of the AA6082 alloy: cast billets and pre-extruded billets, both with a diameter of 49 mm and a length of 75 mm. The chemical composition and the optical microstructure of these materials are presented in Table 1 and Fig. 1, respectively. Both AA6082 billets are within the standard specification range for AA6082. They were sourced from different manufacturers, leading to slight variations in the chemical composition. While the cast billets have been delivered in a homogenized condition, the pre-extruded billets were received in a T6511 temper condition.

Table 1
Chemical compositions of the extrusion billets in wt.-% (Al. in balance).

Billet condition	Mg	Si	Fe	Mn	Ti
Cast	1.10	0.80	0.22	0.50	0.03
Pre-extruded	0.67	0.92	0.20	0.57	0.01

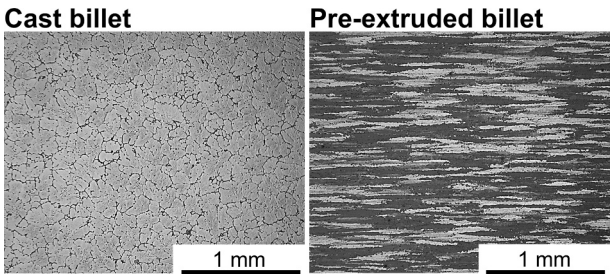

Fig. 1. Microstructure of the initial billet materials in the longitudinal section, with the extrusion direction oriented horizontally.

As a result of the different conditions, the grain structure varies from globular grains with embedded precipitates intragrain and at the grain boundaries in the cast condition to an elongated grain morphology with aligned precipitates in the case of the extruded condition. For the optical microstructure analyses of the billets, the specimens were embedded with the two-component cold mounting medium Demotec 30. Using the semi-automatic grinding/ polishing machine (Saphir 500.3), the samples were ground with fine SiC papers (#800, #1000, #1200 and #2400) for 1 min for each paper and polished with 1 μm diamond suspension and OPS- water free (oxide polishing suspension) for 45 min. To make the grain structure visible, the samples were electrically etched using a Barker solution at an applied voltage of 30 V for 120 s. After etching, the surface was rinsed with distilled water to remove all residues of the etching agent.

Bands with dimensions of 30 mm × 2 mm were extruded using an automated 2.5 MN extrusion press, applying an extrusion ratio of 33 at a constant temperature of 450 °C and a ram speed of 1 mm/s. Two different die geometries were employed in the extrusion trials. First, a conventional die, where the die entrance and exit have the same cross-section, following the shape of the extrudate. Here, the press-channel length is 2.5 mm. Second, a modified die that features a complex press channel geometry enabling the introduction of a positive transverse strain component in the forming zone. This is enforced by a continuous compression in the normal direction (ND) while guiding the material transversally over the press channel length of 14 mm. Further details about this die design are described in an earlier publication [19]. The key geometrical features of each die are highlighted in Fig. 2. While in past studies, the die design was realized by additive manufacturing, in this study, the modified die has been machined by the company WEFA Inotec GmbH (78224 Singen, Germany) from two separate parts. This enables the investigation of the billet remainder and, consequently, the texture development over the extrusion path. After extrusion, the profiles were cooled in ambient air without active water quenching. For the analysis of the billet remainder, the die and the partially extruded material were removed from the press and quenched in a water bath within two minutes after extrusion. This was necessary to prevent further recrystallization driven by the thermal mass of the die steel, which retains heat and can promote microstructural changes in the in-die material.

To analyze the billet remainder regarding microstructure and texture evolution, large-area EBSD measurements (1.15 mm × 0.86 mm) were performed at 100 × magnification using a step size of 0.65 μm. These EBSD measurements were set along the ED/ND cross-section at 4 mm intervals, keeping the ND position of the measurements area near the center and continuing to the end of the billet remainder, see Fig. 2. Grain size was determined using TSL OIM Analysis 7 software. In the case of a globular appearance of the microstructure, a typical equivalent circle diameter method was used to calculate the grain size from EBSD maps, assuming circular grain geometry. In cases with more lamellar microstructures, the major and minor grain shape axis properties are revealed as a representation of the grain structure. Using AztecCrystal software (Oxford Instruments), the fractions of the main texture components

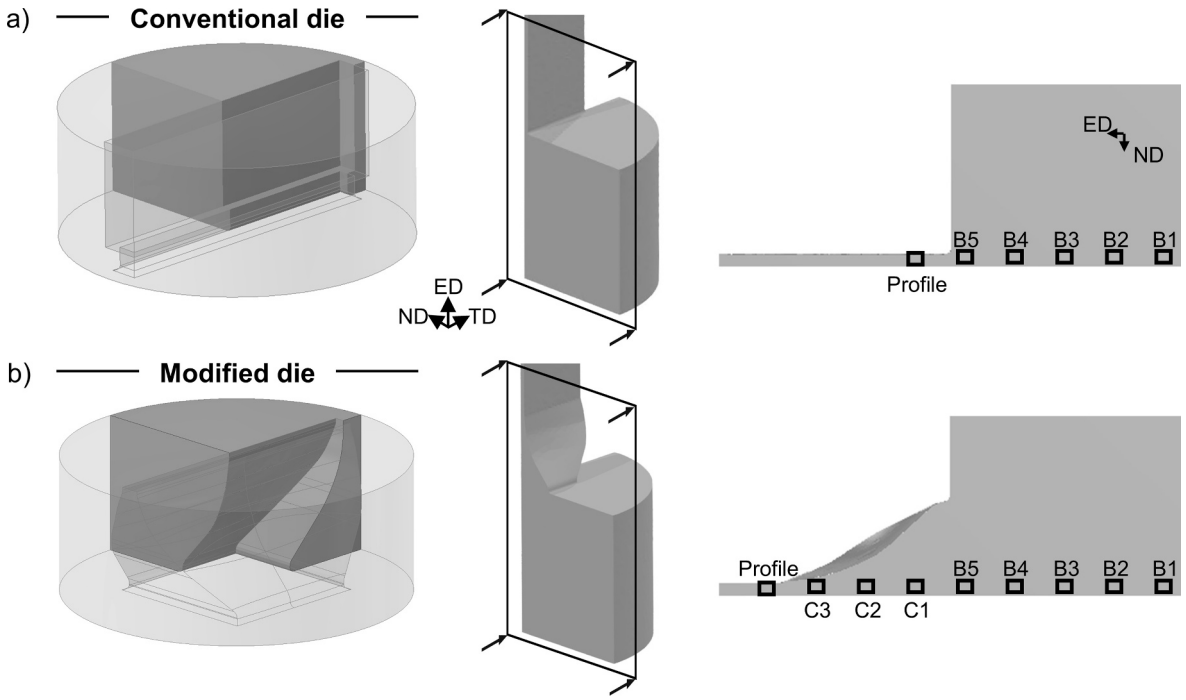

Fig. 2. The three-dimensional model highlighting the key geometrical features, the quarter model of the billet remainder, and the evaluation points set for microstructure and texture analysis and numerical state variable evaluation for a) the conventional and b) the modified die.

(Cube (0,0,0); Goss (0,45,0); Brass (35,49,90); S (59,37,63); Copper (95,35,45)) were quantified based on a misorientation tolerance of 20°. Additionally, a more detailed EBSD scan was performed on the profile using a step size of 0.25 μm at 300 × magnification, covering an area of 0.38 mm × 0.29 mm, to facilitate a more refined microstructural analysis. Recrystallized grains were defined as those exhibiting a grain orientation spread (GOS) of less than 2°, substructured grains as those with GOS values between 2° and 5°, and deformed grains as those with GOS values exceeding 5° [27]. All EBSD measurements were conducted using a ZEISS Crossbeam 550 L scanning electron microscope equipped with an EBSD detector and an accelerating voltage of 20 kV. Due to the complex sample geometry of the billet remainder, they could not be prepared semi-automatically, as was the case with the optical sample preparation of the billets. The billet remainder was ground manually (#1000, #1200 and #2400) for 5–10 min each and then polished with 3 μm diamond suspension for 15 min and 1 μm diamond suspension and OPS-water free (oxide polishing suspension) for 40 min. Finally, a short electro-polishing with "Struers" AC2 solution at − 20 °C and 30 V for 5 s was carried out. Prior to EBSD measurements, the specimens were additionally cleaned using a 0.5 % nitric acid solution to remove surface contamination and ensure optimal pattern quality.

To determine the corresponding mechanical properties of the profiles, uniaxial tensile tests were carried out using a universal testing machine (Z05, Zwick GmbH & Co. KG, Ulm, Germany) with a maximum load capacity of 5 kN. The positioning of the tensile specimens within the extruded band, both in the extrusion direction (ED), transverse direction (TD), and 45°, as well as their geometry, is illustrated in Fig. 3. For each sampling position, three tests were performed at room temperature under a constant initial strain rate of 10^{-3} s^{-1} until fracture. The resulting data were used to generate engineering stress–strain curves. The tensile tests were performed four months after extrusion. During this period, the extruded profiles were stored at room temperature, allowing for natural ageing. This ageing time was consistent across all the conditions investigated.

To correlate the deformation characteristics and recrystallization kinetics present during extrusion to the process-related local state variables, finite element simulations using QForm UK General forming

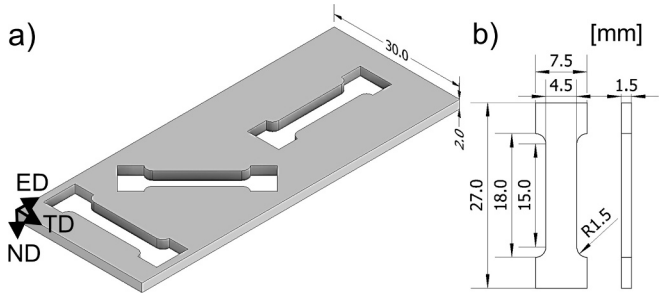

Fig. 3. A) the position of the tensile specimens extracted from the extruded bands and b) their geometry.

module have been carried out. Here, a three-dimensional quarter model of the process is set up, utilizing symmetry planes to reduce numerical complexity. While the die and the container are kept stationary, the ram is displaced at a constant speed of 1 mm/s for 45 mm, thereby ensuring evaluation of stationary state variables in the forming zone. The thermodynamic properties of the tools are sourced from the built-in material library, where conventional H13 tool steel is selected. As the tools are expected to deform slightly and entirely elastically during extrusion, the influence of tool deformation on the state variables in the forming zone will only be minor. Therefore, all tools are modelled as rigid bodies. The elastic deformation of the workpiece is also not considered in the simulation. To capture the plastic behavior of the investigated materials, a series of compression tests was conducted using a hydraulic universal testing machine (ZwickRoell HB250). For the tests, sample cylinders with a height of 17 mm and a diameter of 11 mm were produced vertically from the billets so that the pressure direction is in the ED. To reduce friction between the surfaces of the cylinder and the pressure plates, both surfaces of the specimens were coated with graphite paste (OKS 230) and then covered with graphite foil (diameter 15 mm; thickness 0.13 mm). Each sample was preheated for 5 min at the experimental temperature. The experiments covered a temperature range of 250–450 °C and strain rates between 0.001 s^{-1} and 4 s^{-1},

enabling the generation of flow curves shown in Fig. 4 and Fig. 5 under various thermomechanical conditions. The data for the flow curves are made available online at Zenodo (https://doi.org/10.5281/zenodo.18213558).

A semi-empirical approach is used for the analysis of the correlation between peak flow stress σ_P and a temperature-compensated strain rate Z known as the Zener-Hollomon parameter, following Equation (1) [28–30].

$$Z = \dot{\varepsilon} \bullet \exp\left(\frac{Q}{RT}\right) = A \bullet (\sinh(\alpha \bullet \sigma_P))^n \quad (1)$$

In this case, Q represents an apparent activation energy of the deformation, whereas A, α, and n are fitted material-specific constants. $R = 8.314$ J/(mol•K) represents the universal gas constant. A temperature range of 350–450 °C was chosen to remain near the temperature regime set in this work. The results are collected in Fig. 6.

The friction stresses τ are incorporated into the simulation model based on the formulation by Levanov [31] given by:

$$\tau = m\left(\frac{\sigma_F}{\sqrt{3}}\right)\left(1 - \exp\left(-1.25\frac{\sigma_C}{\sigma_F}\right)\right) \quad (2)$$

where $m = 1$ represents the friction factor, σ_F is the flow stress of the material, and σ_C is the contact stress between the workpiece and the tool. The model is validated based on a comparison of the resulting ram load as the mechanical response of the entire system, see Fig. 7.

The model shows high agreement with the experimentally obtained ram load–displacement curve and is therefore considered validated. To evaluate the influence of the billet condition and the die design on deformation and recrystallization behavior of the materials, the strain tensor $\varepsilon \in \mathbb{R}^{3\times3}$, strain rate $\dot{\varepsilon}$, and the temperature T are evaluated using the post-processor and standard subroutines available in QForm UK. Additionally, a subroutine is implemented into the QForm UK environment, which, based on these state variables, enables the calculation of von Mises equivalent strain ε_{vM} as given by:

$$\varepsilon_{vM} = \sqrt{\frac{2}{9}[(\varepsilon_1 - \varepsilon_2)^2 + (\varepsilon_2 - \varepsilon_3)^2 + (\varepsilon_3 - \varepsilon_1)^2]} \quad (3)$$

with ε_1, ε_2, and ε_3 as the principal strains.

3. Results and Discussion

3.1. Microstructure and texture development

Fig. 8 and Fig. 9 illustrate the microstructure and texture evolution from the billet remainder (positions "B1-B5") to the final profile using both the conventional and the modified die for the cast billets. Due to its increased press channel length, the strain path of the modified die is extended. Therefore, it also includes analysis regions within the die ("C1-C3"). Texture evolution is represented using orientation distribution functions (ODFs) at $\varphi_2 = 0°$ and 45°. Additionally, the volume fractions of the main texture components at the measured positions are presented in Fig. 10.

For both the conventional and the modified die, microstructural analysis at position B1 revealed a typical cast structure characterized by coarse, globular grains with an average grain size of approximately 155 µm, averaging both cases. For the conventional die, first small grain morphological changes can already be observed at position B2. However, strong deformation with elongation of grains along ED became evident at position B3. For the modified die, the elongation already starts at position B2 and gets more pronounced at B3. At B3, the longitudinal grain elongation is more distinct in the specimen extruded with the conventional die. From this point onward, differences in microstructural evolution depending on the die geometry are apparent. At B4, the conventional die shows further grain elongation and thinning, while the formation of smaller, globular grains along the elongated grains is observed only at B5, just before entry of the die exit into the final profile.

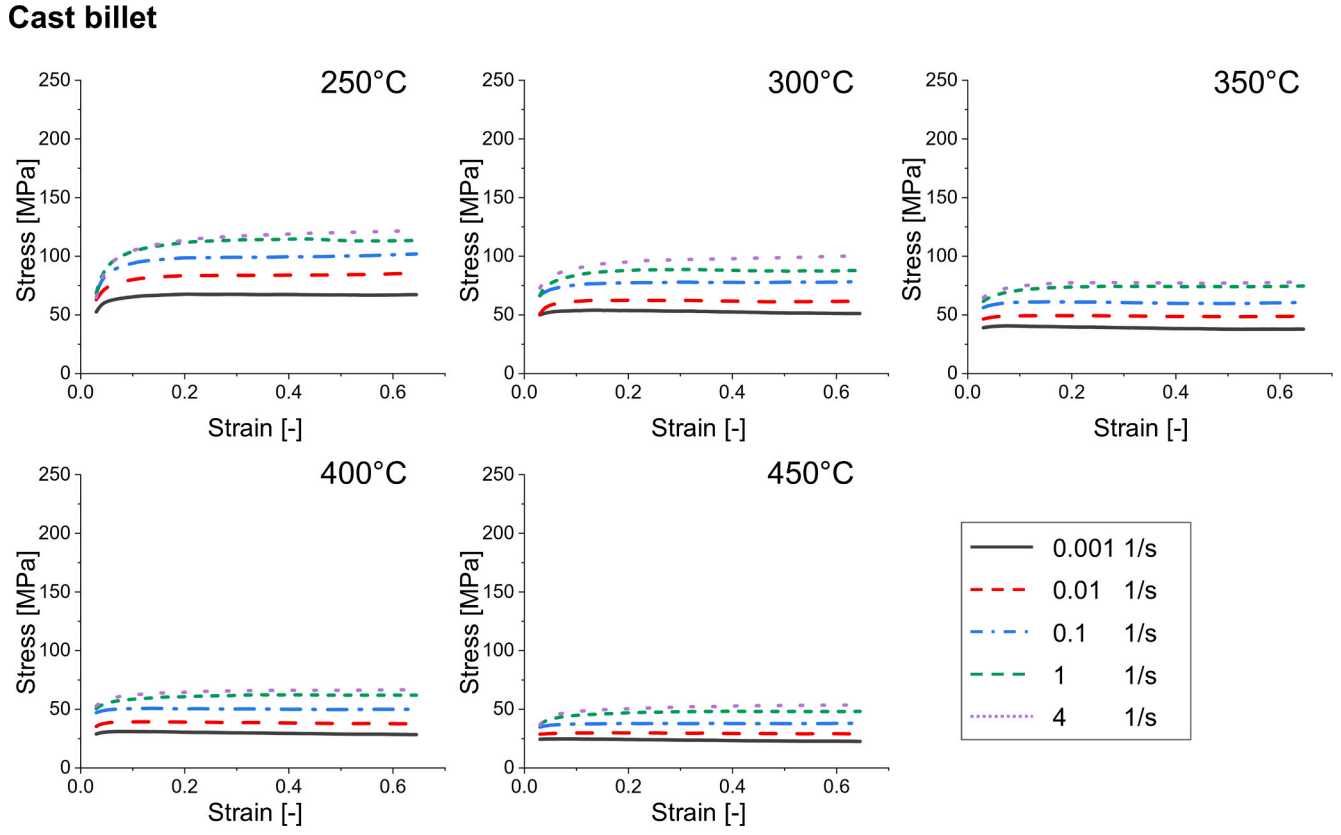

Fig. 4. Interpolated true stress–strain curves from AA6082 cast billets.

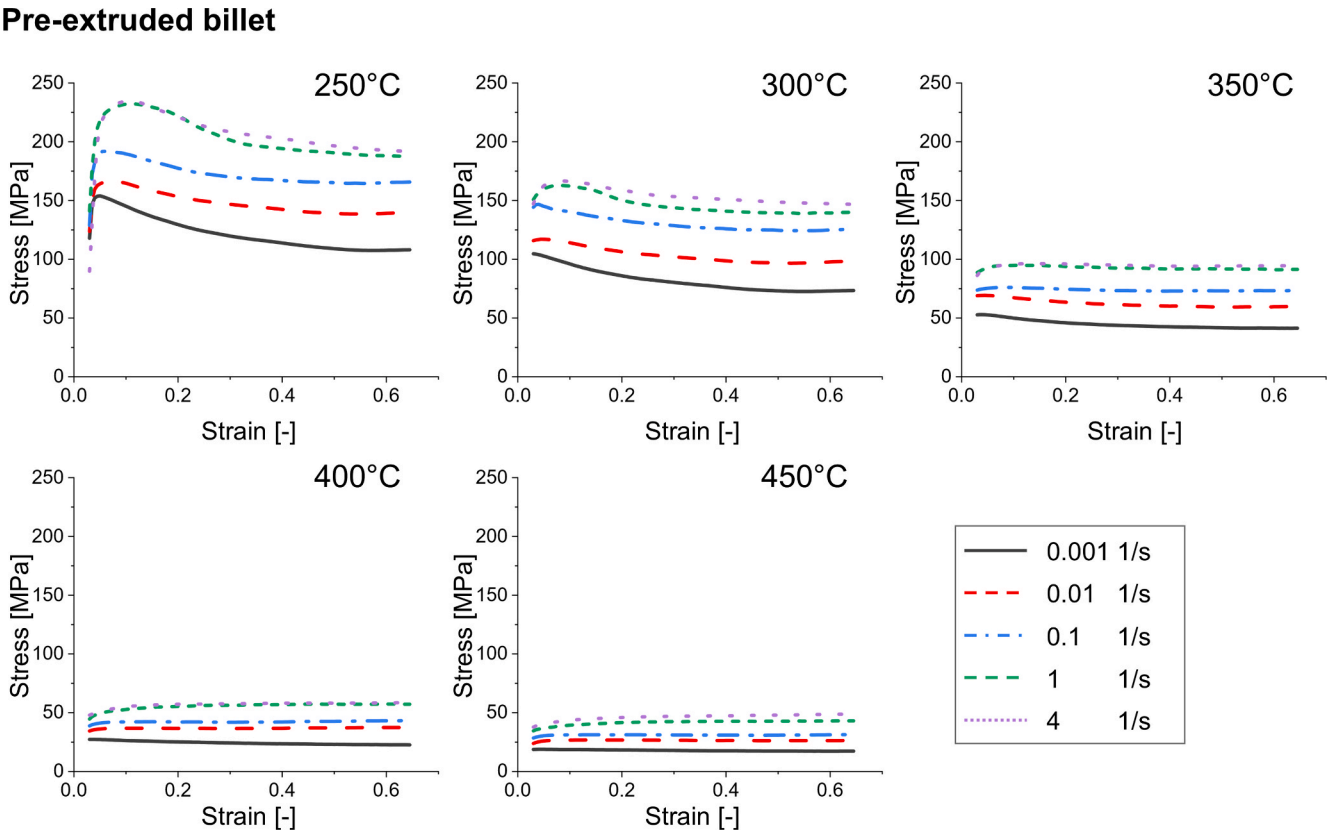

Fig. 5. Interpolated true stress–strain curves from pre-extruded AA6082 billets.

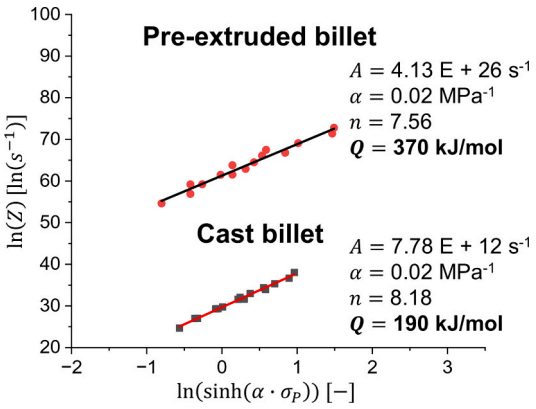

Fig. 6. Zener-Hollomon fit for the identification of the material-specific constants.

In contrast, the modified die exhibits significant grain thinning and elongation not until entering the chamber (C1), but the formation of new globular grains occurs already at B3. The positions C2 and C3 in the modified die continue to show grain refinement and the emergence of small globular grains. In the final profile, both extruded bands exhibit a band-like microstructure with very similar lamellar width of ca. 3.6 μm and length of the lamellas in the form of the major grain shape axis of 31 μm in the case of the conventional die (Fig. 8) and 42 μm in the case of the modified die (Fig. 9). However, only the band processed with the conventional die shows a PCG zone.

The texture evolution is shown by the ODF sections at $\varphi_2 = 0°$ and 45° and collected by the volume fractions of the main texture components at the measured positions (see Fig. 10). Both die designs exhibit a typical random texture characteristic of the as-cast condition at B1. As the extrusion progresses, a continuous increase in deformation texture components is observed, as the Brass component intensifies up to the profile, while the Copper component develops continuously from B2 until B4 in the conventional die and from B3 until B5 in the modified die. It is evident that there is a significant decline in the magnitude of the Copper component within the press channel of the modified die, see C1-C3. Additionally, the conventional die shows a rise in the S component up to B4, followed by a subsequent decline. Recrystallization texture components, such as Cube and Goss, remain relatively weak when extruding with the conventional die. However, Cube is slightly more pronounced. In the modified die, Goss is significantly more evident, particularly in the final profile, with the Cube component being almost unobservable. In both cases, the final texture in the profile is dominated by deformation texture components. While in the conventional die, Brass and Copper are the prevailing components, with minor contributions from S and Cube, in the modified die, Brass remains dominant, accompanied by lower fractions of Copper and Goss.

These observations highlight a clear difference in recrystallization behavior between the two different die geometries. The earlier appearance of globular grains and the presence of Goss in the modified die suggest that dynamic recrystallization initiates sooner and that the Goss component may be developed through the recrystallization of cube bands, as also suggested by Chen et al. [14].

As for the pre-extruded billet extruded with the conventional die (see Fig. 11) and the modified die (see Fig. 12), the microstructural evolution clearly shows the typical elongated grain structure in the billet remainder (B1), characteristic of extruded materials, with elongated grains somewhat along ED and an average major grain shape axis of 278 μm whereas the thickness of the lamellas averages at 24 μm (minor grain shape axis). However, for the modified die, the angle of the grains at position B1 appears slightly different, possibly connected to variations in the material flow characteristics of the two investigated dies. In position B2 for the modified die and B3 for the conventional die, grain

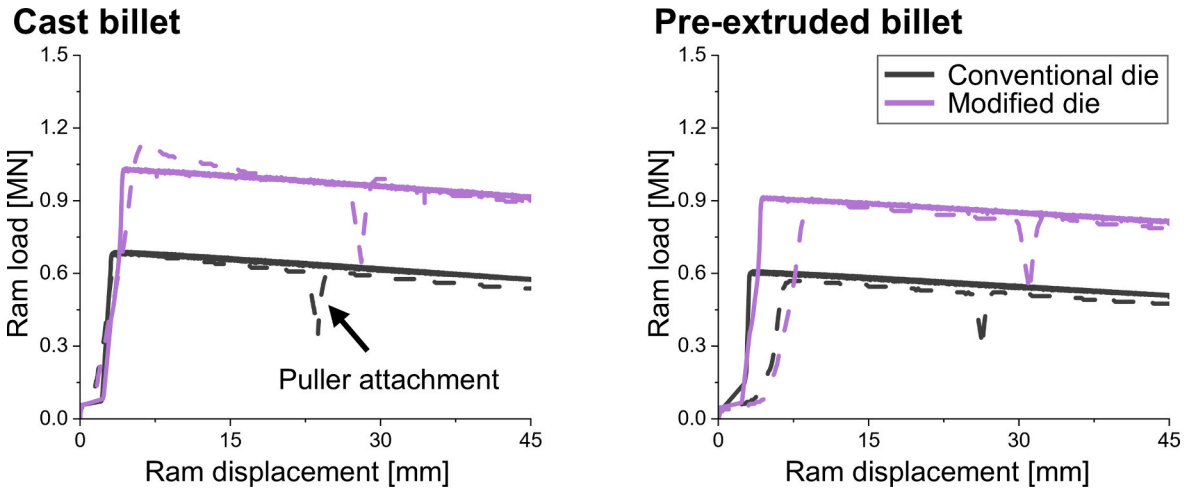

Fig. 7. Comparison of experimental (dashed line) and simulated (solid line) ram load–displacement curves.

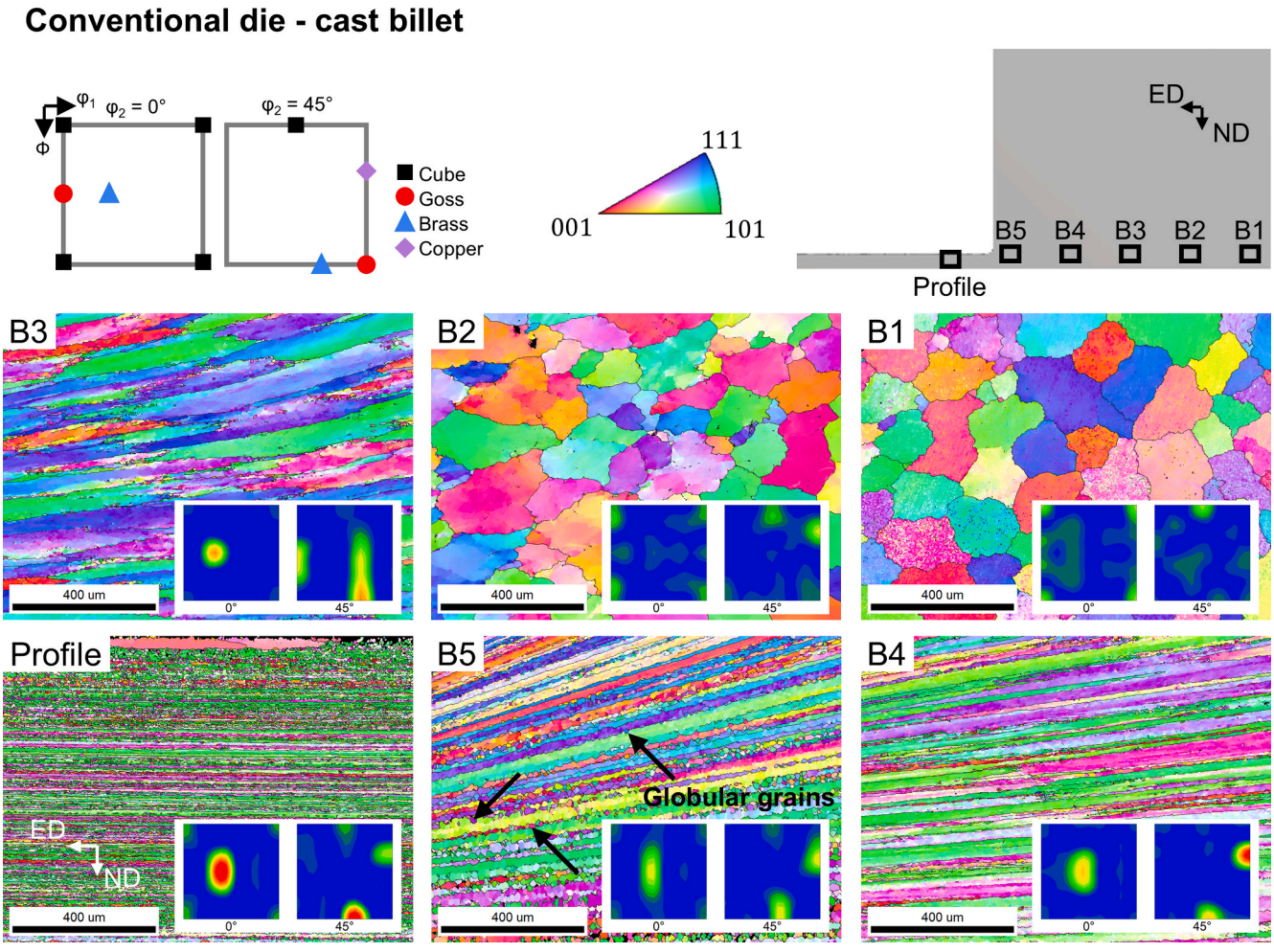

Fig. 8. Microstructure and texture evolution using the conventional die with the cast billet. The arrows mark the occurrence of globular grains following the elongation. Longitudinal section with ED aligned horizontally, and IPF EBSD maps with TD chosen as the sample reference axis for color coding.

refinement through grain thinning occurs, although the elongated grains remain clearly visible. In the modified die, specifically, the formation of small globular grains along elongated grains can already be observed from B3 onward, whereas in the conventional die, this phenomenon appears only partially from position B4. Similar to the extrusion experiments conducted with cast billets, the recrystallization behavior appears to be influenced by the die. At stage B5, before the material begins to flow into the respective die, the conventional die appears to exhibit a greater number of newly formed globular grains. Then, in the final profile, the material extruded through the conventional die shows significant recrystallization, also forming a PCG zone with a thickness of 132 μm. In the modified die, particularly in stages C1 to C3, a

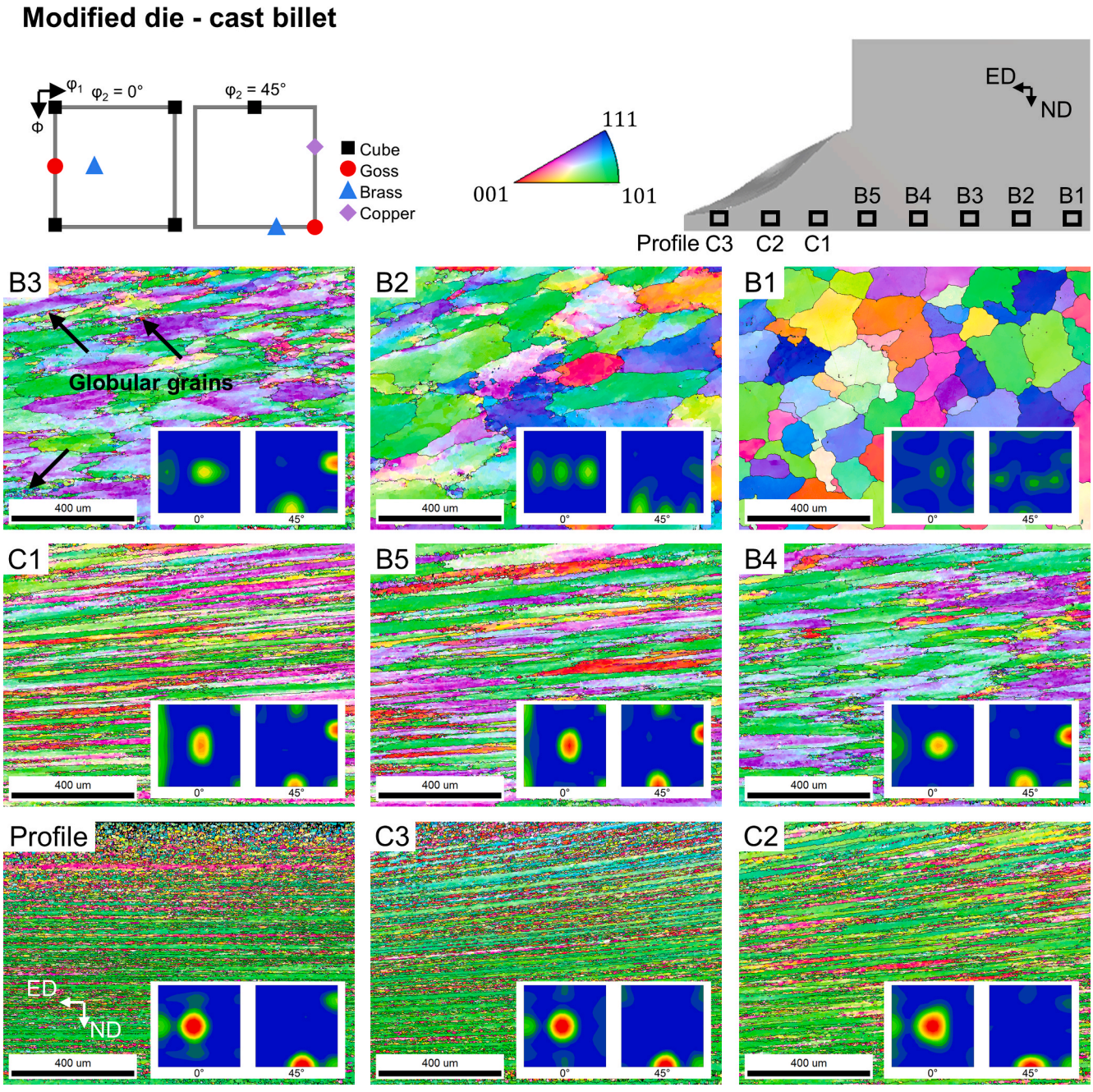

Fig. 9. Microstructure and texture evolution using the modified die with the cast billet. The arrows mark the occurrence of globular grains following the elongation. Longitudinal section with ED aligned horizontally, and IPF EBSD maps with TD chosen as the sample reference axis for color coding.

pronounced grain refinement and further formation of small globular grains along the longitudinal stretched grains can be observed, which is assumed to result from GDRX [32,33]. In the final profile, the microstructure does not show a PCG zone. The formation mechanism of the PCG zone remains an active topic of current research, particularly in aluminum extrusion. While earlier studies have identified high local strain and elevated stored energy as key drivers for PCG development [25,34,35], recent investigations have expanded the understanding of how die geometry, strain path, and thermomechanical conditions influence this phenomenon. Negozio et al. [25] and Wang et al. [35] demonstrated that die bearing geometry and strain gradients significantly affect PCG formation, with smoother strain paths reducing PCG formation. Sun et al. [36] and Mahmoodkhani et al. [26] emphasized the influence of dynamic recrystallization and surface strain localization on the formation of PCG. Goik et al. [37] further showed that the PCG layer grows into the fine-grained bulk when grain boundary mobility is low, and that Cube-oriented grains can counteract this growth if their mobility is sufficiently high. The findings suggest that the modified die mitigates the conditions that typically favor PCG formation. Despite these differences, both bands exhibit a similar grain structure with a minor grain shape axis of 3.3–3.4 μm, whereas the major grain shape axis is slightly higher at 13.6 μm in the profile extruded with the conventional die (Fig. 11) when compared to the profile extruded using the modified die at 9.2 μm (Fig. 12).

The differences in recrystallization play a key role in the final texture formation of the bands. The texture data shown by the volume fractions of the main texture components at the measured positions (Fig. 13) reveal that the initial regions (B1–B3) in both extrusion routes are characterized by a high fraction of deformation-related components, including Copper, as well as recrystallization-related components, such

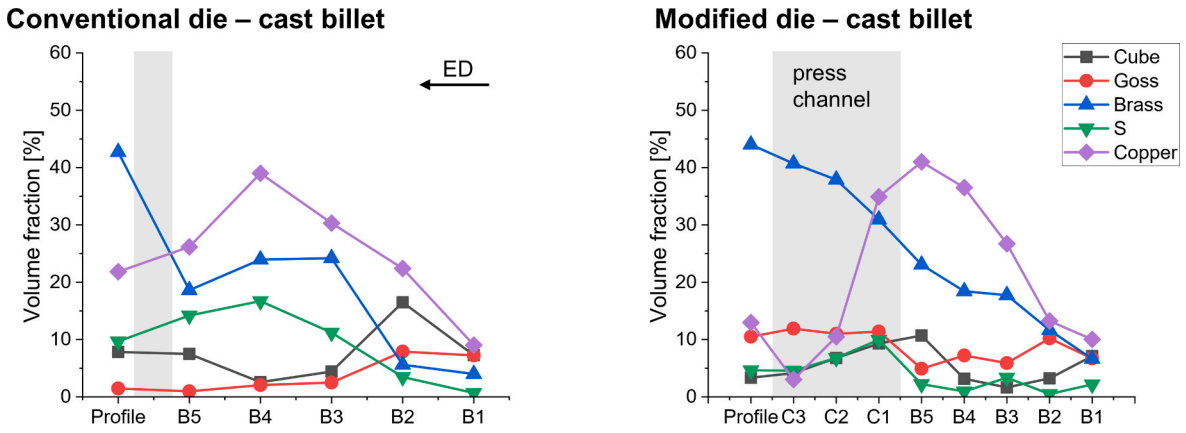

Fig. 10. Fraction of main texture components using the conventional and modified die with cast billets.

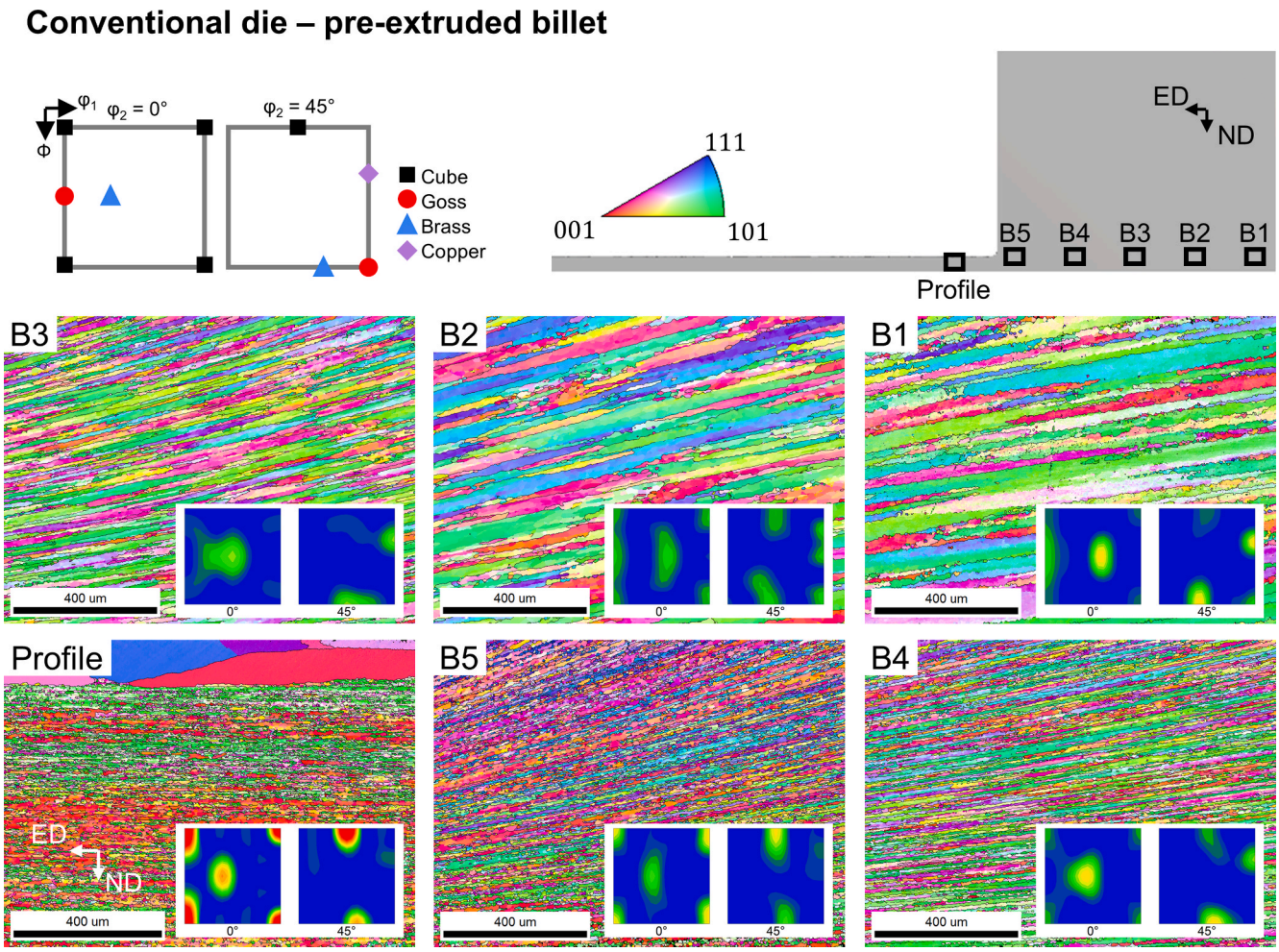

Fig. 11. Microstructure and texture evolution using the conventional die with the pre-extruded billet. Longitudinal section with ED aligned horizontally, and IPF EBSD maps with TD chosen as the sample reference axis for color coding.

as Cube and Goss. Clear differences compared to the cast billets are evident. The extruded billets already exhibit a pronounced initial texture, consisting of both deformation and recrystallization components. In the conventional die, the transition from deformation to recrystallization is marked by a sharp increase in the Cube component from B4 to the final profile. This is accompanied by a decline in the Copper component, while the Brass component remains relatively stable. In contrast, the modified die shows a more gradual evolution, with the Goss component becoming dominant only after the material passes through the press channel (C1–C3). Here, a significant decrease in the Copper component is also observed, which, in turn, increases again from stage C2 to the final profile. The Cube component initially forms but appears to diminish from C2 onward in favor of Copper and Goss.

Overall, while in the profile extruded with the conventional die, the texture is dominated by Cube and a minor Brass component, the profile extruded with the modified die is characterized by multifold texture

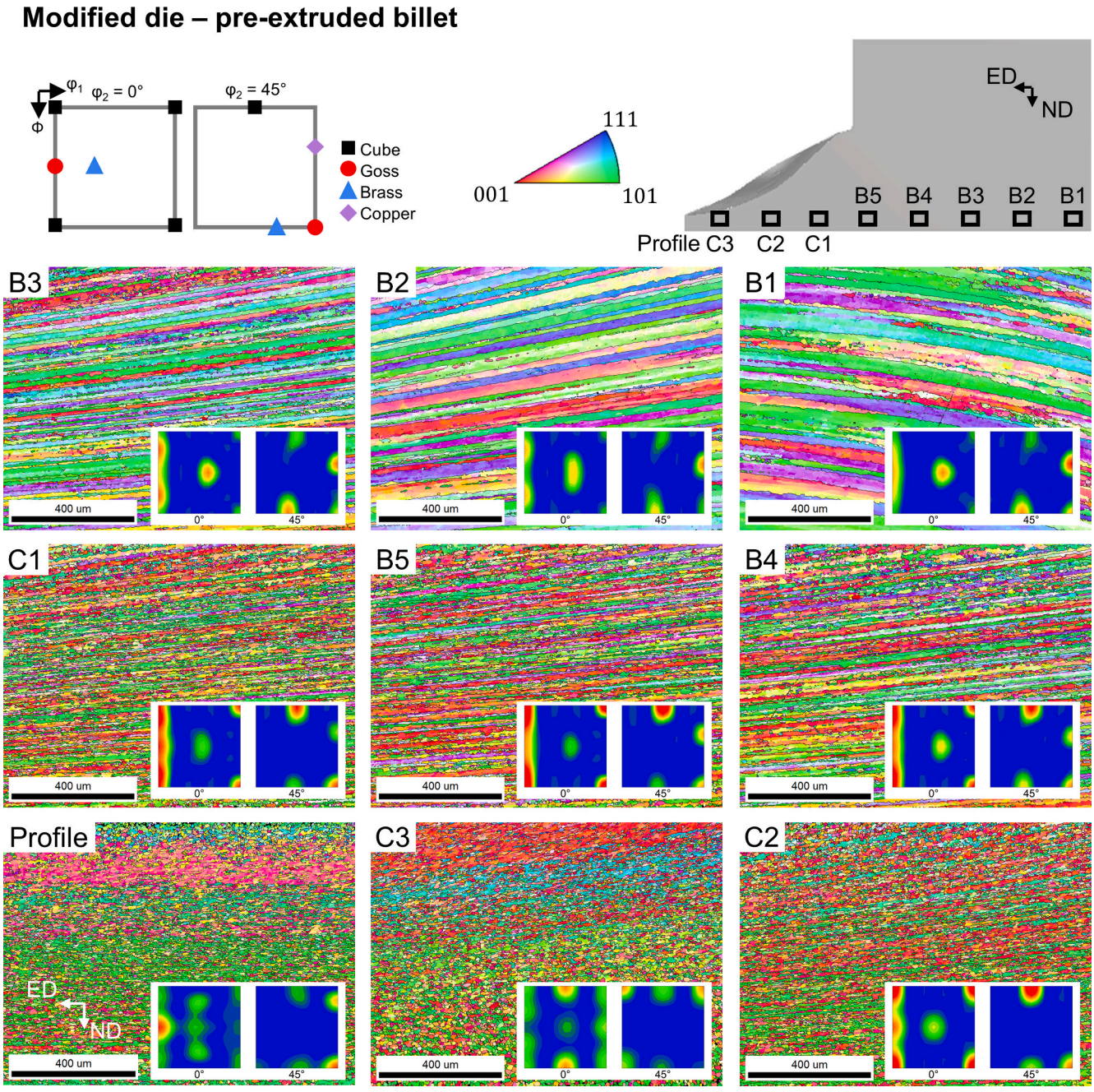

Fig. 12. Microstructure and texture evolution using the modified die with the pre-extruded billet. Longitudinal section with ED aligned horizontally, and IPF EBSD maps with TD chosen as the sample reference axis for color coding.

components: a dominant Goss component, along with a mixture of Copper, Brass, and Cube components. However, with either die, the final profiles exhibit a recrystallization texture, dominated either by the Cube component (conventional die) or the Goss component (modified die). This suggests that the modified die not only alters the strain path but also creates conditions that accelerate the nucleation and growth of recrystallized grains. Notably, it promotes the development of Goss-oriented grains at the expense of Cube-oriented ones. This shift suggests a competitive relationship between the two texture components, which is influenced by the local deformation and recrystallization kinetics. Cube texture typically forms through primary recrystallization due to its low stored energy and favorable subgrain structure [12,13]. In contrast, Goss texture is often associated with secondary recrystallization and selective grain growth in shear bands, where grains with higher mobility and growth advantage dominate [15,16]. According to Chen et al. [14], Goss-oriented grains can emerge from Cube bands under specific conditions, such as elevated stored energy or strain localization. Liu et al. [38] and Kestens et al. [39] further emphasize that Cube and Goss grains may originate from distinct substructures and compete during recrystallization, depending on the thermomechanical environment. Recent studies have expanded this understanding by showing that Goss grains preferentially grow along Σ9 coincidence site lattice (CSL) boundaries, while Cube grains grow along Σ5 boundaries, with their mobility being strongly temperature-dependent [40]. The presence of CSL boundaries and their interaction with dispersoids and precipitates can significantly influence which texture component dominates [41]. Additionally, particle-stimulated nucleation (PSN) has been shown to promote Goss texture development in Al–Cu–Mg alloys, especially when particles are finely dispersed and aligned with shear bands [40,42]. Finally, deformation temperature has a significant impact on the

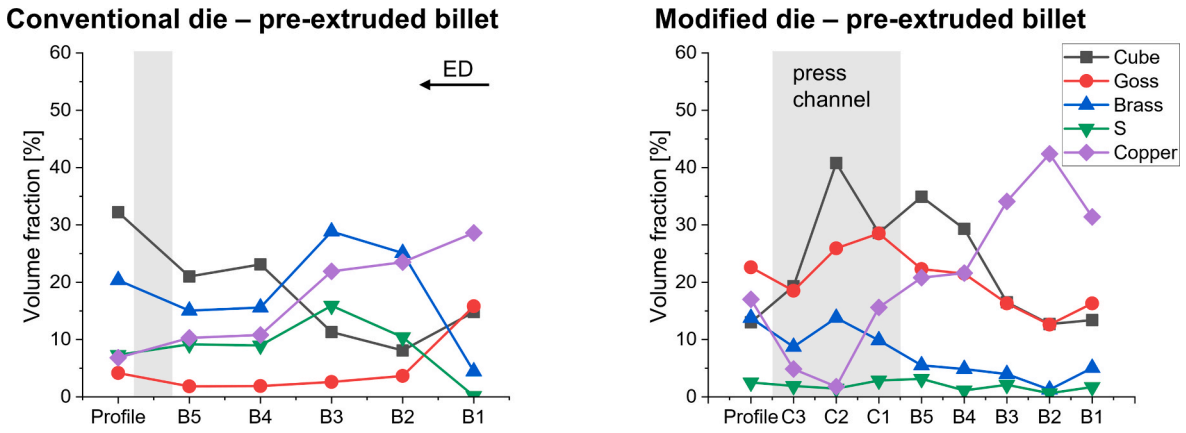

Fig. 13. Fraction of main texture components using the conventional and modified die with pre-extruded billet.

mechanical properties and grain refinement behavior of Al–Mg alloys, which in turn affects the development of recrystallization textures such as Cube and Goss [43]. These findings support the hypothesis that the modified die, by extending the strain path, promotes conditions favorable for Goss texture development, such as elevated stored energy, shear localization, CSL boundary mobility, and PSN activity, thereby suppressing Cube texture formation and altering the final texture outcome.

To substantiate the observed differences in deformation and recrystallization behavior between the two dies and billet conditions, von Mises equivalent strain ε_{vM}, strain rate $\dot{\varepsilon}$, and temperature T are numerically evaluated, as shown in Fig. 14. To this end, points are placed in the simulation model within the measurement areas highlighted in Fig. 2.

As deformation is characteristic of the material flow, ε_{vM} and $\dot{\varepsilon}$ are approximately the same for both billet conditions, with only slight deviations originating from numerical instabilities. However, the simulation further reveals that the strains introduced using the conventional die increase until B5, just before entry of the die, and then remain roughly the same in the profile. Especially between B3 and B5, the incline in ε_{vM} is significant, as the strain is increased from about 1.5 to 3.0. Correspondingly, $\dot{\varepsilon}$ increases starting at about B3 and reaches its maximum just before entry of the conventional die with about 11 s^{-1}. These results are in good agreement with the microstructural analysis of cast and pre-extruded billets, where deformation is observed to begin at B3, then significantly increases until B5, see Fig. 8 and Fig. 11.

Using the modified die, the introduction of strains is smoother, gradually increasing ε_{vM} from about 1.0 at B1 to 3.0 at C1. However, within the modified press channel, ε_{vM} is slightly reduced. This reduction in ε_{vM} can be attributed to the reduction of the strain in the extrusion direction ε_{ED} between C2 and C3, while, between the same positions, the strain in the transverse direction ε_{TD} changes from compression to tension, see Fig. 15. The results suggest a through-thickness variation of underlying strain states, limiting the meaningfulness of ε_{vM} for the evaluation of the strain state, due to the complexity of the strain tensor achieved with the modified die. As for the $\dot{\varepsilon}$, an increase is already present at B2, indicating earlier introduction of strain than with the conventional die. This observation corresponds well with the microstructure analysis, also showing a beginning of deformation at B2, especially highlighted with the cast billet, see Fig. 9. Despite

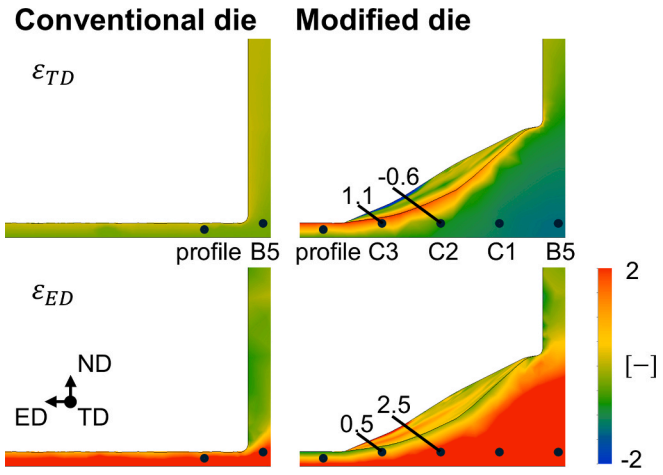

Fig. 15. Strain distribution in TD and ED in the ND-ED cross section for the conventional and the modified die design.

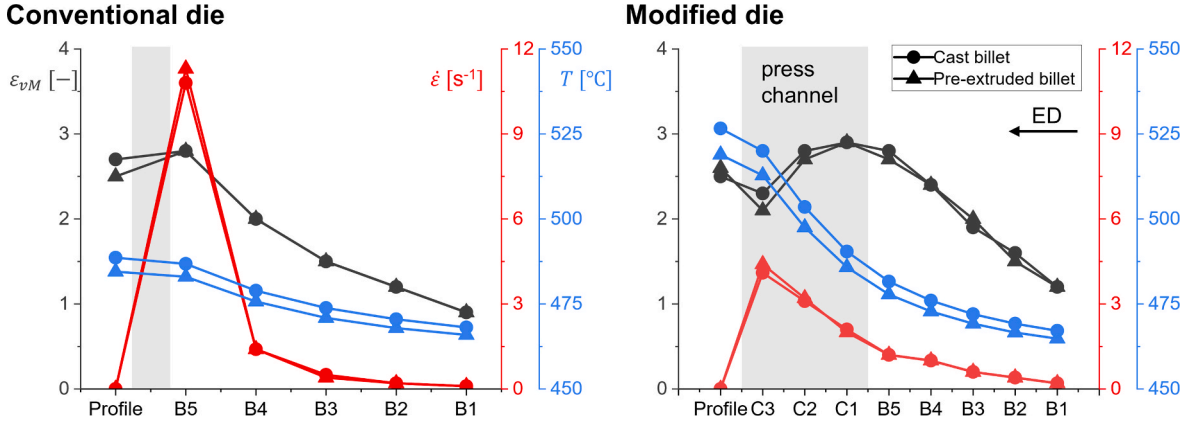

Fig. 14. Evolution of von Mises equivalent strain, strain rate, and temperature using the conventional and modified die.

increasing earlier, the strain rate remains lower from B4 onwards when compared to the conventional die. The maximum reached is only about 4 s^{-1}, however, the strain rate is kept at an increased level for a longer space/time interval. Regarding the microstructure development, the grains also elongate more gradually, most notably for the cast billet, where deformation dominates the microstructure. These differences in strain introduction are also reflected in the texture development. While the rapid introduction of strains using the conventional die is associated with a mixture of deformation texture components, here Brass, Copper, and S, the smoothed introduction of strains using the modified die correlates with the gradual intensification of the Brass component, see Fig. 10. Regarding these differences in deformation textures, the results of the pre-extruded billet are less conclusive, as the recrystallization overlays the texture development more extensively.

Due to the increased friction and the prolonged deformation associated with the modified die design, heat generation during extrusion is increased. Consequently, temperatures in the profile reach about 519–527 °C, which are substantially higher than those obtained with the conventional die at about 485–489 °C. Despite these differences in thermomechanical conditions, the microstructures do not exhibit significant differences concerning the grain axis dimensions between the two different die designs. However, a clear distinction is observed regarding the dominant recrystallization texture present, as either the Cube or the Goss component dominates depending on the used die. This increase in forming temperature, combined with the reduction in strain rate, effectively lowers the Zener Hollomon parameter Z (see equation (1)), which appears to be correlated with a favoured formation of the Goss component over the Cube component. Hence, the recrystallization kinetics, and consequently the recrystallization textures, are distinctly influenced by the die design.

With respect to the billet condition, only minor differences are observed in the forming temperatures reached, with the cast billet showing marginally higher temperatures calculated by the simulation. This is clearly associated with the slightly higher flow stresses observed for the cast billet under the applied extrusion conditions, which is experimentally reflected by the higher maximum ram load compared to that of the pre-extruded billet, see Fig. 7. Notably, the experimentally determined activation energy Q for the pre-extruded billet is higher than that obtained for the cast billet, consistent with the temperature sensitivity of the flow curves obtained through hot compression tests. This difference in Q itself is significant, often associated with variations in chemical composition [44] and/or the presence of precipitates [45]. While the significantly higher Q of the pre-extruded billet indicates increased resistance to dislocation motion at lower temperatures, it also highlights the rapid decline of flow stresses with increasing temperatures [28], see Fig. 16.

This temperature sensitivity of the pre-extruded billet condition suggests that the mechanisms responsible for strengthening at lower temperatures may facilitate enhanced softening at elevated temperatures, such as through dynamic recrystallization. As the simulation results report temperatures well above 450°C, those effects are believed to promote accelerated recrystallization kinetics in the pre-extruded billet when compared to the cast billet, which appears to be less sensitive to the forming temperature. This finding is also supported by the observed differences in grain morphology and texture development of the pre-extruded billet after extrusion, indicative of altered recrystallization behavior.

In summary, the cast material exhibits slower and less efficient microstructural refinement and development of recrystallized texture components during extrusion compared to the pre-extruded material. These differences highlight the importance of the initial billet condition in controlling recrystallization kinetics and texture evolution, which are crucial for tailoring the mechanical properties of extruded products. This suggests that the cast material requires higher strain accumulation to activate effective nucleation mechanisms. The lack of a well-developed subgrain structure in the cast billets delays the onset of recrystallization and leads to a broader distribution of deformed texture components. This behavior is consistent with findings in aluminum alloys, where substructure-controlled nucleation is strongly influenced by the initial grain morphology and dislocation density [46,47].

3.2. Mechanical properties

For each processing condition, the mechanical properties are evaluated regarding three orientations, namely in ED, in TD, and at 45° in between, as shown in Fig. 17. In Table 2, the tensile yield strength (TYS), the ultimate tensile strength (UTS), and the fracture strain are summarized.

Significant differences in mechanical properties are observable during extrusion trials using cast billets, depending on the type of die employed. By extrusion through a conventional die, pronounced anisotropic behavior in terms of UTS, with values of 169 MPa in the ED and TD, and a reduced value of 148 MPa at 45° orientation, are obtained. The TYS ranged between 78–86 MPa, while fracture strain varied from 24–28 %. In contrast, the use of the modified die leads to a reduction in anisotropy for UTS, with 177 MPa in ED, 187 MPa in TD, and 175 MPa in 45°. No significant differences in TYS are found when compared to the conventional die, with values ranging from 80–89 MPa. However, a marginal increase in elongation is noted, ranging from 23–29 %. This significant influence of the die on mechanical properties is also evident in trials using pre-extruded billets. The conventional die results in UTS values between 161–172 MPa. Here, the modified die

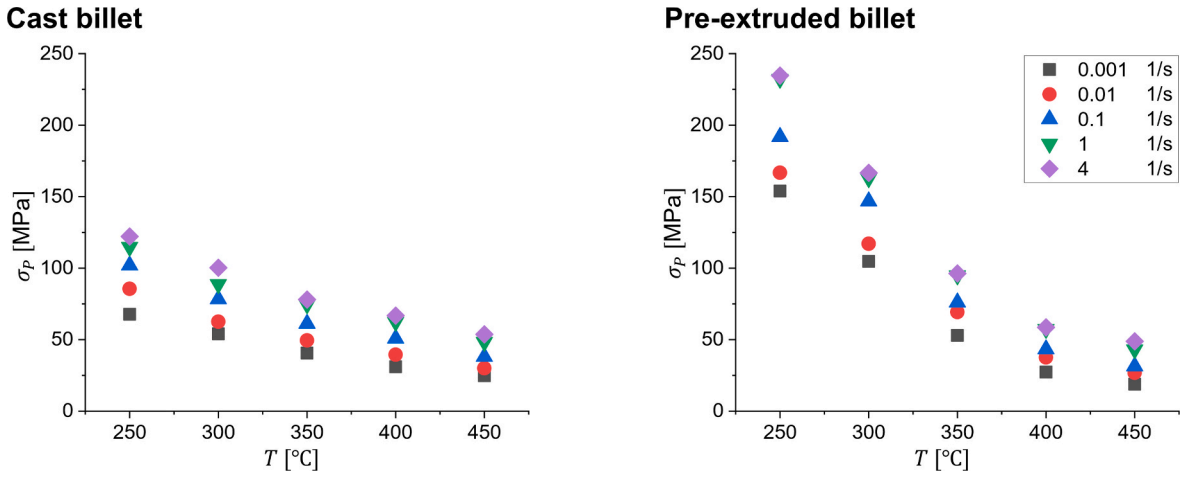

Fig. 16. Peak flow stress σ_P of the pre-extruded and cast billet at varying temperatures and strain rates, obtained through hot compression tests.

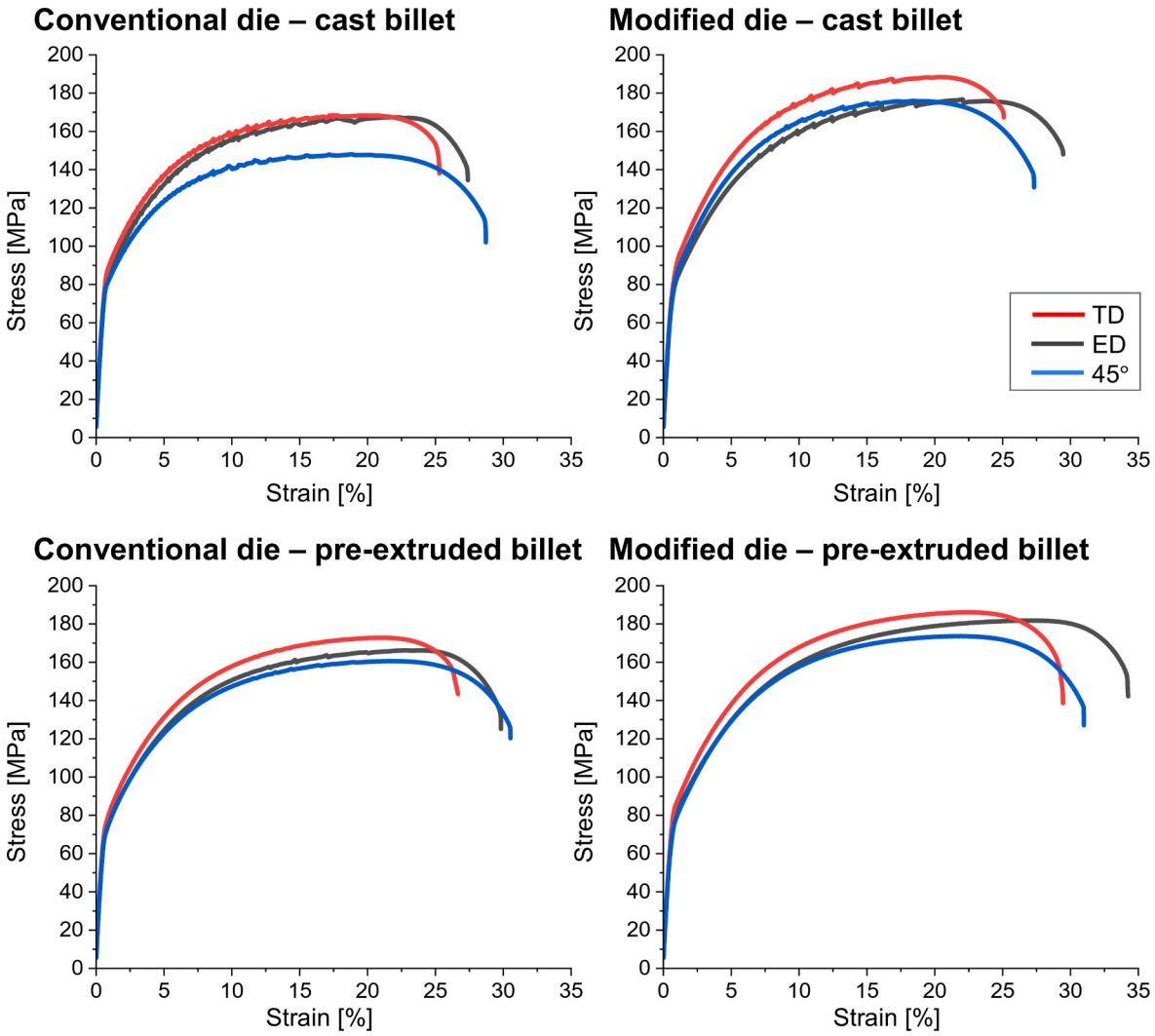

Fig. 17. Stress–strain curves for AA6082 under different processing conditions and orientations.

leads to an increase in strength, with UTS values ranging from 174–186 MPa, while no strong directional dependence was observed. For the conventional die, TYS varied between 71–75 MPa, indicating the lowest anisotropy in TYS among all tested conditions. The modified die caused a slight increase in TYS to 75–83 MPa, accompanied by a slight rise in anisotropy. Elongation values ranged from 25–30 % for the conventional die and increased to 29–33 % for the modified die.

Fig. 18 illustrates the trends in TYS, UTS, and fracture strain across all processing conditions and orientations. It highlights the superior performance of the modified die, particularly in terms of ductility, and the trade-off between strength and elongation in cast versus pre-extruded billet conditions. The visual representation confirms that the modified die leads to a more balanced mechanical response, especially when used with pre-extruded billets.

A local texture analysis near the location of extraction of tensile specimens is shown in Fig. 19, thereby enabling a correlation of mechanical properties with microstructure, degree of deformation, recrystallization, and the final texture developed. As with the billet remainder analyses, the texture reveals that different components dominate in the respective bands. For cast billets, the use of the conventional die leads to domination of Brass and Copper components. Using the modified die, Brass and Goss are most pronounced. By selecting the pre-extruded billet and extruding with the conventional die, Cube, Brass, and Copper components can be found, while using the modified die, Goss, Brass, and Copper components are dominant.

As texture refers to the preferred orientation of grains within the polycrystalline material, the texture components are decisive for the mechanical response and the anisotropy. Related work suggests that Brass and Copper are often associated with high strength and limited ductility, typically resulting in anisotropic material behavior [39,48]. This is clearly reflected in the present results. Particularly for cast billet conditions, a pronounced directional dependence of mechanical properties is observed for the profile extruded with the conventional die, however, significantly reduced with the modified die. In contrast, recrystallization textures like Cube and Goss promote more isotropic behavior, contributing to uniform strength and ductility across directions [49,50]. Yet, the Cube component, due to its orientation, contributes to a softer material [51]. This correlates well with the TYS found for the profile of pre-extruded billet and conventional die design. Using the modified die and selecting the pre-extruded billet, Goss component is dominant, thereby improving both the UTS and ductility of the profiles. This observation has been supported, as Goss orientation can be advantageous for achieving high strength combined with good ductility [52,53].

Correspondingly, a clear trend is observed: while the fraction of deformation texture components decreases, the fraction of recrystallization texture components increases when selecting the pre-extruded billet over the cast billet and choosing the modified die over the conventional die. This trend aligns with the microstructural evolution, as indicated by the GOS analysis. The fraction of grains with GOS $\leq 2°$,

Table 2
Mechanical properties from tension tests parallel to ED, TD and 45° (tensile yield stress (TYS), ultimate tensile stress (UTS)) with standard deviations.

Billet condition	Die design	Specimen	TYS (MPa)	UTS (MPa)	Fracture strain (%)
Cast	Conventional die	ED	81 ± 1	169 ± 2	25.6 ± 1.4
		TD	86 ± 1	169 ± 1	24.0 ± 0.6
		45°	78 ± 2	148 ± 1	27.7 ± 0.4
	Modified die	ED	80 ± 2	177 ± 3	28.5 ± 0.5
		TD	**89 ± 1**	**187 ± 2**	22.8 ± 1.2
		45°	83 ± 2	175 ± 1	26.2 ± 0.3
Pre-extruded	Conventional die	ED	71 ± 1	166 ± 1	29.1 ± 1.1
		TD	75 ± 1	172 ± 1	25.1 ± 0.6
		45°	71 ± 1	161 ± 1	29.8 ± 0.3
	Modified die	ED	77 ± 3	180 ± 6	**33.1 ± 0.6**
		TD	83 ± 1	**186 ± 1**	28.5 ± 0.2
		45°	75 ± 1	174 ± 1	29.7 ± 0.2

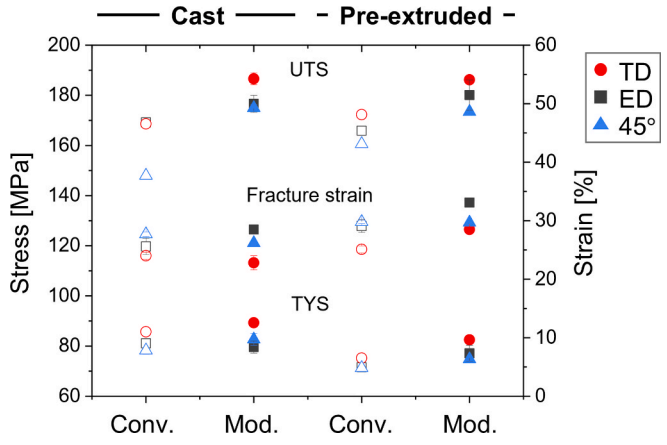

Fig. 18. Summary of mechanical properties (TYS, UTS, and fracture strain) for AA6082. Hollow markers indicate the properties obtained with the conventional die (Conv.), while the solid markers indicate the properties obtained with the modified die (Mod.).

indicative of fully recrystallized grains, is highest in the pre-extruded condition of the modified die (45.7 %), followed by the pre-extruded condition of the conventional die (35.4 %), the cast condition of the modified die (27.7 %), and lastly the cast condition of the conventional die (20.3 %). These fractions of recrystallization correlate well with the observed mechanical properties, as higher degrees are associated with improved ductility, lower TYS, and a more uniform mechanical response. Recent studies have demonstrated that dynamic recrystallization mechanisms, particularly CDRX and GDRX, contribute significantly to the reduction of mechanical anisotropy in aluminum and magnesium alloys. The homogenization of grain orientation and refinement through DRX promotes more isotropic mechanical behavior. This is consistent with findings by Kareem et al. [3] and Li et al. [54] who observed improved ductility and reduced directional dependence in extruded alloys due to enhanced recrystallization kinetics. In addition to the increased fraction of recrystallized grains, the grain morphology in the pre-extruded condition with the modified die is notably more equiaxed. This uniform grain shape contributes to the reduction in mechanical anisotropy, as equiaxed grains facilitate more homogeneous deformation behavior across different loading directions. This observation is consistent with findings by Tomé et al. [55], who demonstrated that equiaxed grain structures in recrystallized aluminum alloys reduce in-plane anisotropy due to more uniform strain accommodation.

In addition to microstructure and texture, alloying elements also influence properties and, most significantly, recrystallization behavior. The chemical composition (Table 1) of the cast and pre-extruded billets shows notable differences, particularly in the concentrations of Mg, Si, and Mn. While both materials fall within the standard specification range for AA6082, these variations can influence recrystallization kinetics, precipitation behavior, and texture evolution. Magnesium increases stored energy and stabilizes substructures, thereby delaying recrystallization through solute drag effects [56–58]. In this study, the cast billets with higher Mg content (1.10 wt-%) show reduced recrystallization compared to the pre-extruded billets (0.67 wt-%), consistent with literature findings. The Mn content is slightly higher in the pre-extruded billets (0.57 wt-%) than in the cast billets (0.50 wt-%). Manganese contributes to recrystallization resistance via the formation of α-Al(MnFe)Si dispersoids, which pin grain boundaries and inhibit nucleation [59–61]. However, despite slightly higher Mn content in the pre-extruded billets, enhanced recrystallization is observed, suggesting that Mn does not dominate the kinetics. The Si content is also slightly higher in the pre-extruded billets (0.92 wt-%) compared to the cast billets (0.80 wt-%). Increased Si content promotes particle-stimulated dynamic recrystallization during hot extrusion [62]. Overall, the observed differences in microstructure and texture between the two billet conditions are likely the result of a complex interplay between initial microstructure and thermomechanical history, with chemical composition playing a secondary role.

In summary, the mechanical performance of AA6082 is strongly influenced by both the die design and the billet condition, as substantial differences are found in the microstructure, e.g. the degree of recrystallization, and the texture developed. Extrusion of cast billets, while generating profiles with higher TYS, shows reduced ductility and higher mechanical anisotropy. The modified die enhances strength and ductility across all directions, particularly when pre-extruded billets are used, as a mixture of recrystallization and deformation texture components can be found. Therefore, the mechanical performance of AA6082 is strongly influenced by both the die design and the billet condition, and the interplay between them. These findings underscore the importance of actively selecting billet conditions and, correspondingly, die design to achieve tailored mechanical properties in extruded aluminum profiles.

4. Conclusions

This study provides a comprehensive analysis of the microstructure–property relationships in extruded AA6082 flat bands, emphasizing the combined influence of billet condition and die design. By analyzing the billet remainder alongside the final profiles, the progression of texture development along the extrusion path was revealed. It was demonstrated that the billet condition significantly affects recrystallization behavior, texture evolution, and mechanical performance, and that this change can further be altered using the die design. The key findings can be summarized as follows:

- The billet condition significantly influences recrystallization and texture evolution. Pre-extruded billets promote finer, more homogeneous grain structures and higher fractions of Cube and Goss texture components, resulting in improved ductility and reduced anisotropy compared to cast billets.
- The die design alters strain path and recrystallization kinetics. The modified die enables smoother strain introduction over a longer

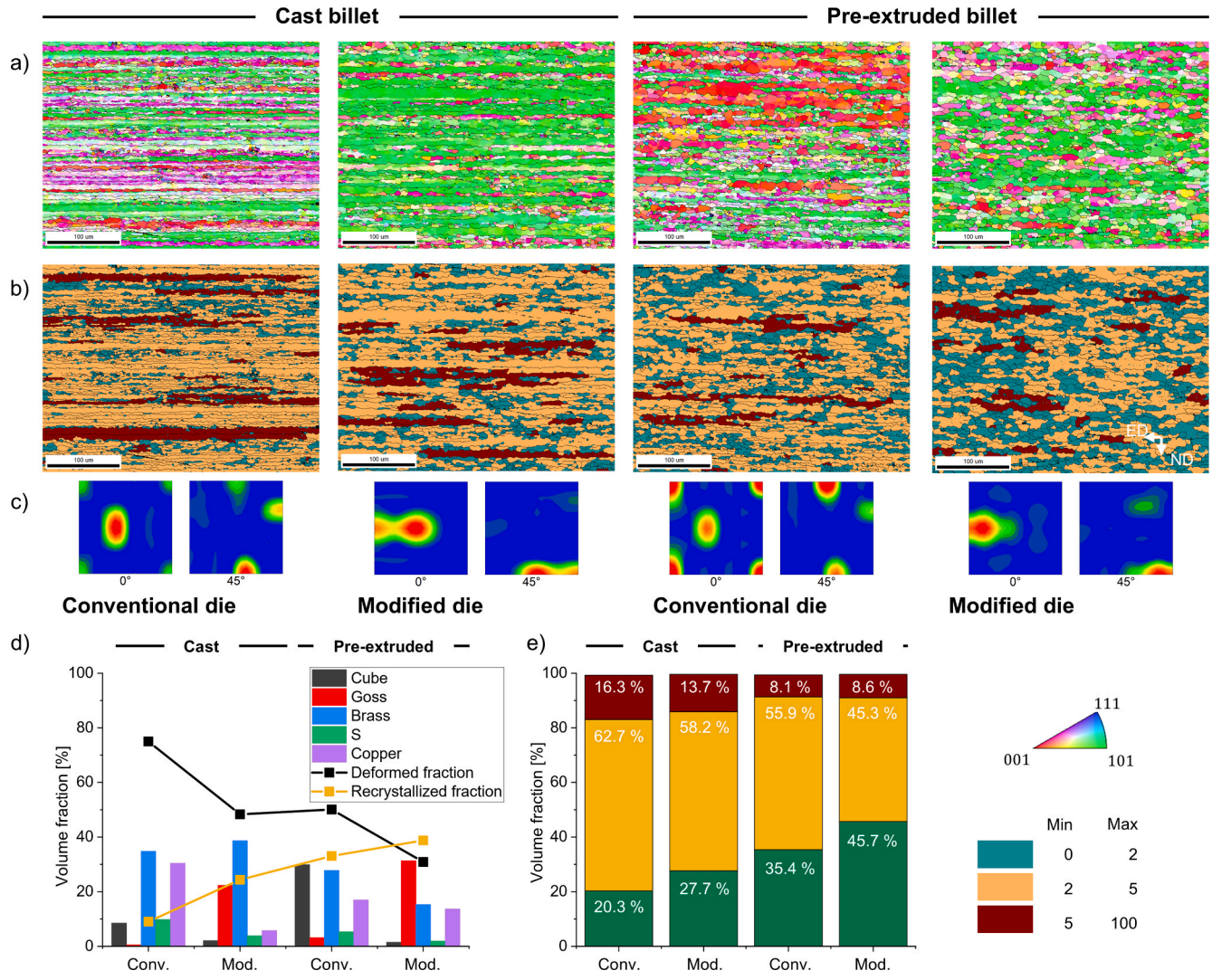

Fig. 19. Detailed EBSD analysis of longitudinal section near the tensile specimens with ED aligned horizontally and IPF EBSD maps with TD chosen as the sample reference axis for color coding: a) IPF-map; b) subdivision of microstructural fractions into grain orientation spread; c) ODF for 0° and 45°; d) volume fraction of the main texture components; e) percentages of different grain type (Recrystallized grains are classified as having GOS values less than 2°, substructured grains are classified as having GOS values of 2-5° and deformed grains are classified as having GOS values more than 5°).

interval, possibly facilitating dynamic recrystallization, suppressing peripheral coarse grain formation, and promoting Goss orientation.

- Mechanical performance is optimized by combining pre-extruded billets with the modified die. This combination yields the highest ultimate tensile strength, uniform elongation, and minimal directional dependence, making it ideal for lightweight structural applications.

In conclusion, the analysis of the billet remainder was essential for understanding the origin and evolution of the recrystallization textures of AA6082. The findings highlight that both initial microstructure and strain path engineering via die design are key to tailoring texture and mechanical properties in aluminum extrusion. The insights gained from this study offer valuable guidance for industrial extrusion practices, particularly in applications where mechanical performance and anisotropy control are critical.

CRediT authorship contribution statement

Maria Nienaber: Writing – original draft, Visualization, Validation, Methodology, Investigation, Formal analysis, Conceptualization. **Fabian Esterl:** Writing – original draft, Visualization, Validation, Methodology, Investigation, Formal analysis, Conceptualization. **Noomane Ben Khalifa:** Writing – review & editing, Supervision, Project administration, Funding acquisition. **Jan Bohlen:** Writing – review & editing, Supervision, Project administration, Funding acquisition, Formal analysis.

Declaration of competing interest

The authors declare that they have no known competing financial interests or personal relationships that could have appeared to influence the work reported in this paper.

Acknowledgments

The research has been funded by the Deutsche Forschungsgemeinschaft (DFG, German Research Foundation) under the project number: 455039650.

Data availability

The obtained flow curve data of this research are online available at Zenodo (https://doi.org/10.5281/zenodo.18213558). The other data

will be made available upon request.

References

[1] H.J. McQueen, W. Blum, *Dynamic recovery: sufficient mechanism in the hot deformation of Al (<99.99)*, Mater. Sci. Eng. A 290 (1–2) (2000) 95–107, https://doi.org/10.1016/S0921-5093(00)00933-3.

[2] P. Sun, R. Huang, L. Wan, Y. Zhang, S. Zheng, X. Yuan, M. Li, *Contribution of dynamic recrystallization mechanism to the transformation of orientation preference in Al-Mg-Si alloy*, Scr. Mater. 268 (2025), https://doi.org/10.1016/j.scriptamat.2025.116889.

[3] S.A. Kareem, J.U. Anaele, E.O. Aikulola, O.F. Olanrewaju, B.O. Omiyale, S. O. Falana, S.R. Oke, M.O. Bodunrin, *Hot deformation behavior of aluminum alloys: a comprehensive review on deformation mechanism, processing maps analysis and constitutive model description*, Mater. Today Commun. 44 (2025), https://doi.org/10.1016/j.mtcomm.2025.112004.

[4] A. Zang, J.-F. Béland, A. Khajezade, N. Parson, W.J. Poole, *Localization of plastic deformation at weld seams of porthole die Al-Mg-Si extrusions*, Mater. Sci. Eng. A 943 (2025), https://doi.org/10.1016/j.msea.2025.148781.

[5] M. Khadyko, C.D. Marioara, S. Dumoulin, T. Børvik, O.S. Hopperstad, *Effects of heat-treatment on the plastic anisotropy of extruded aluminium alloy AA6063*, Mater. Sci. Eng. A 708 (2017) 208–221, https://doi.org/10.1016/j.msea.2017.09.133.

[6] Zhang, K., Holmedal, B., Hopperstad, O.S., and Dumoulin, S., *Modelling the plastic anisotropy of aluminum alloy 3103 sheets by polycrystal plasticity*. Modelling and Simulation in Materials Science and Engineering, 2014. **22**(7). DOI: 10.1088/0965-0393/22/7/075015.

[7] T. Manik, K. Marthinsen, K. Zhang, A.I. Aria, B. Holmedal, *Deformation Texture Evolution in Flat Profile AlMgSi Extrusions: Experiments, FEM, and Crystal Plasticity Modeling*, Front. Mater. 8 (2021), https://doi.org/10.3389/fmats.2021.636379.

[8] C.-H. Cho, D.-O. Kim, K. Son, H.-S. Park, *Relationship between hot workability and texture evolution in an Al–Zn–Mg–Cu alloy under hot compressive stress mode*, J. Mater. Sci. 58 (42) (2023) 16537–16549, https://doi.org/10.1007/s10853-023-09081-3.

[9] O. Engler, *Correlating crystallographic texture with anisotropic properties and sheet metal forming of aluminium alloys*, J. Mater. Res. Technol. 35 (2025) 514–522, https://doi.org/10.1016/j.jmrt.2025.01.059.

[10] L. Fu, G. Wu, C. Zhou, Z. Xiu, W. Yang, J. Qiao, *Effect of Microstructure on the Dimensional Stability of Extruded Pure Aluminum*, Materials (basel) 14 (17) (2021), https://doi.org/10.3390/ma14174797.

[11] X. Duan, H. Jiang, Z. Mi, L. Cheng, J. Wang, *Reduce the Planar Anisotropy of AA6016 Aluminum Sheets by Texture and Microstructure Control*, Crystals 10 (11) (2020), https://doi.org/10.3390/cryst10111027.

[12] I. Samajdar, R.D. Doherty, Role of S [(123)<634>] orientations in the preferred nucleation of cube grains in recrystallization of fcc metals, Scr. Metall. Mater. 32 (6) (1995) 845–850, https://doi.org/10.1016/0956-716X(95)93212-M.

[13] J. Hjelen, R. Ørsund, E. Nes, *On the origin of recrystallization textures in aluminium*, Acta Metall. Mater. 39 (7) (1991) 1377–1404, https://doi.org/10.1016/0956-7151(91)90225-P.

[14] J. Chen, W.J. Poole, N.C. Parson, *The effect of through thickness texture variation on the anisotropic mechanical response of an extruded Al-Mn-Fe-Si alloy*, Mater. Sci. Eng. A 730 (2018) 24–35, https://doi.org/10.1016/j.msea.2018.05.105.

[15] L.F. Shuai, T.L. Huang, G.L. Wu, X. Huang, O.V. Mishin, *Development of Goss texture in Al–0.3%Cu annealed after heavy rolling*, J. Alloy. Compd. 749 (2018) 399–405, https://doi.org/10.1016/j.jallcom.2018.03.187.

[16] T. Omura, Y. Hayakawa, *Influence of Primary-Recrystallization Texture on Selective growth of Goss grains*, Mater. Trans. 54 (1) (2013) 14–21, https://doi.org/10.2320/matertrans.M2012303.

[17] Ghosh, A., Elasheri, A., Parson, N., and Chen, X.G., *Microstructure and texture evolution during high-temperature compression of Al-Mg-Si-Zr-Mn alloy*. Materials Characterization, 2023. **205**. DOI: 10.1016/j.matchar.2023.113312.

[18] Y. Li, G. Zhao, L. Sun, B. Zhang, X. Zhao, *Texture evolution induced by extrusion parameters and its effect on strengthening-toughening mechanisms of Al-Mg-Si-Cu-Mn alloys*, Mater. Sci. Eng. A 916 (2024), https://doi.org/10.1016/j.msea.2024.147377.

[19] F. Esterl, M. Nienaber, J. Bohlen, N. Ben Khalifa, *Connecting texture development to die design in extruded flat products*, J. Manuf. Process. 134 (2025) 891–903, https://doi.org/10.1016/j.jmapro.2024.12.078.

[20] N. Ben Khalifa, J. Isakovic, J. Bohlen, *New concepts of extrusion dies to reduce the anisotropy of extruded profiles by means of additive manufacturing*, CIRP Ann. 70 (1) (2021) 231–234, https://doi.org/10.1016/j.cirp.2021.04.006.

[21] Y. Wang, A. Zang, Y. Mahmoodkhani, M. Wells, W. Poole, N. Parson, *The effect of Bridge Geometry on Microstructure and Texture Evolution during Porthole die Extrusion of an Al–Mg–Si–Mn–Cr Alloy*, Metall. Mater. Trans. A 52 (8) (2021) 3503–3516, https://doi.org/10.1007/s11661-021-06322-5.

[22] A. Zang, Y. Wang, A. Khajezade, N. Parson, M. Wells, W.J. Poole, *The development of crystallographic texture during porthole die extrusion of Al-Mg-Si alloys*, Mater. Des. 248 (2024), https://doi.org/10.1016/j.matdes.2024.113468.

[23] B. Ma, L. Liu, Y. Guo, X. Xu, L. Zhang, G. Wu, X. Tong, S. Pang, F. Qi, *Effects of extrusion ratio and temperature on microstructure and mechanical properties of extruded Al-4Cu-1Li-0.4Mg-0.4Ag-0.11Zr alloy*, Mater. Today Commun. 47 (2025), https://doi.org/10.1016/j.mtcomm.2025.112989.

[24] S. Li, I.J. Beyerlein, M.A.M. Bourke, *Texture formation during equal channel angular extrusion of fcc and bcc materials: comparison with simple shear*, Mater. Sci. Eng. A 394 (1–2) (2005) 66–77, https://doi.org/10.1016/j.msea.2004.11.032.

[25] M. Negozio, S. di Donato, R. Pelaccia, A.H.A. Lutey, D. Carosi, B. Reggiani, A. Morri, L. Donati, *Impact of die design and bearing geometry on grain size and PCG formation during extrusion of AA6082 aluminum alloy*, Journal of Materials Science & Technology 230 (2025) 80–92, https://doi.org/10.1016/j.jmst.2025.01.017.

[26] Y. Mahmoodkhani, J. Chen, M.A. Wells, W.J. Poole, N.C. Parson, *The effect of die Bearing Geometry on Surface Recrystallization during Extrusion of an Al-Mg-Si-Mn Alloy*, Metall. Mater. Trans. A 50 (11) (2019) 5324–5335, https://doi.org/10.1007/s11661-019-05437-0.

[27] G. Chen, K. Wu, Y. Wang, Y. Sun, X. Wang, Z. Zhu, F. Hu, *Quantitative study on the correlation between microstructure and mechanical properties of additive friction stir deposited 6061-T6 Al-Mg-Si alloy*, J. Mater. Res. Technol. 25 (2023) 6725–6736, https://doi.org/10.1016/j.jmrt.2023.07.097.

[28] H.J. McQueen, N.D. Ryan, *Constitutive analysis in hot working*, Mater. Sci. Eng. A 322 (2002) 43–63, https://doi.org/10.1016/S0921-5093(01)01117-0.

[29] L. Zhang, X. Wu, X. Zhang, X. Yang, Y. Li, *Constitutive Model and Recrystallization Mechanism of Mg-8.7Gd-4.18Y-0.42Zr Magnesium Alloy during Hot Deformation*, Materials (basel) 15 (11) (2022), https://doi.org/10.3390/ma15113914.

[30] J. Liu, Z. Cui, C. Li, *Modelling of flow stress characterizing dynamic recrystallization for magnesium alloy AZ31B*, Comput. Mater. Sci 41 (3) (2008) 375–382, https://doi.org/10.1016/j.commatsci.2007.04.024.

[31] A.N. Levanov, *Improvement of metal forming processes by means of useful effects of plastic friction*, J. Mater. Process. Technol. 72 (1997) 314–316, https://doi.org/10.1016/S0924-0136(97)00191-X.

[32] R.D. Doherty, D.A. Hughes, F.J. Humphreys, J.J. Jonas, D.J. Jensen, M.E. Kassner, W.E. King, T.R. McNelley, H.J. McQueen, A.D. Rollett, *Current issues in recrystallization: a review*, Mater. Sci. Eng. A 238 (2) (1997) 219–274, https://doi.org/10.1016/S0921-5093(97)00424-3.

[33] J.-K. Chang, K. Takata, K. Ichitani, E.M. Taleff, *Abnormal Grain growth and Recrystallization in Al-Mg Alloy AA5182 following Hot Deformation*, Metall. Mater. Trans. A 41 (8) (2010) 1942–1953, https://doi.org/10.1007/s11661-010-0213-7.

[34] M. Negendank, U.A. Taparli, S. Gall, S. Muller, W. Reimers, *Microstructural evolution of indirectly extruded seamless 6xxx aluminum tubes with axial variable wall thickness*, J. Mater. Process. Technol. 230 (2016) 187–197, https://doi.org/10.1016/j.jmatprotec.2015.11.024.

[35] Y. Wang, G. Zhao, X. Xu, X. Chen, *Exploring Impact of die Structure on Peripheral Coarse Grain Formation and Mechanical Properties of 2195 Al–Cu–Li Alloy Extrusion Plates*, Metall. Mater. Trans. A 56 (9) (2025) 3621–3647, https://doi.org/10.1007/s11661-025-07865-7.

[36] Y. Sun, X. Bai, D. Klenosky, K. Trumble, D. Johnson, *A Study on Peripheral Grain Structure Evolution of an AA7050 Aluminum Alloy with a Laboratory-Scale Extrusion Setup*, J. Mater. Eng. Perform. 28 (8) (2019) 5156–5164, https://doi.org/10.1007/s11665-019-04208-7.

[37] P. Goik, A. Schiffl, H.W. Höppel, *Formation of Peripheral Coarse Grain in Thin-Walled Al–Mg–Si Extrusion Profiles*, Metall. Mater. Trans. A 54 (10) (2023) 3940–3956, https://doi.org/10.1007/s11661-023-07144-3.

[38] J. Liu, Y. Sha, K. Hu, F. Zhang, L. Zuo, *Formation of Cube and Goss Texture after Primary Recrystallization in Electrical Steels*, Metall. Mater. Trans. A 45 (1) (2013) 134–138, https://doi.org/10.1007/s11661-013-1917-2.

[39] L.A.I. Kestens, H. Pirgazi, *Texture formation in metal alloys with cubic crystal structures*, Mater. Sci. Technol. 32 (13) (2016) 1303–1315, https://doi.org/10.1080/02670836.2016.1231746.

[40] Q. Zhao, Z. Liu, S. Bai, S. Li, Y. Hu, P. Xia, *Coincidence site lattice boundary mechanism for the preferred growth of Goss and Cube grains during annealing in an Al-Cu-Mg alloy*, Mater Charact 141 (2018) 193–211, https://doi.org/10.1016/j.matchar.2018.04.030.

[41] Q. Zhao, Z. Liu, Y. Hu, S. Li, S. Bai, *Evolution of Goss texture in an Al–Cu–Mg alloy during cold rolling*, Arch. Civ. Mech. Eng. 20 (1) (2020), https://doi.org/10.1007/s43452-020-00023-3.

[42] Q. Zhao, Z. Liu, *Formation and development of Goss texture in Al–Cu–Mg alloy during solution treatment*, J. Mater. Sci. 58 (35) (2023) 14220–14244, https://doi.org/10.1007/s10853-023-08836-2.

[43] D. Singh, P.N. Rao, R. Jayaganthan, *Effect of deformation temperature on mechanical properties of ultrafine grained Al–Mg alloys processed by rolling*, Mater. Des. 50 (2013) 646–655, https://doi.org/10.1016/j.matdes.2013.02.068.

[44] X. Qian, N. Parson, X.G. Chen, *Effects of Mn addition and related Mn-containing dispersoids on the hot deformation behavior of 6082 aluminum alloys*, Mater. Sci. Eng. A 764 (2019), https://doi.org/10.1016/j.msea.2019.138253.

[45] S. Spigarelli, E. Evangelista, H.J. McQueen, *Study of hot workability of a heat treated AA6082 aluminum alloy*, Scr. Mater. 49 (2) (2003) 179–183, https://doi.org/10.1016/S1359-6462(03)00206-9.

[46] T. Furu, H.E. Vatne, *Grain Structure Control of Flat Extruded AA6082 Alloy*, Mater. Sci. Forum 331–337 (2000) 843–848, https://doi.org/10.4028/www.scientific.net/MSF.331-337.843.

[47] Q. Yang, T. Wojcik, E. Kozeschnik, *A dislocation-based model for the substructure evolution and flow stress of aluminum alloys during high-temperature compression*, J. Mater. Res. Technol. 35 (2025) 4520–4533, https://doi.org/10.1016/j.jmrt.2025.02.132.

[48] M. Miraglia, P. Dawson, T. Leffers, *On the influence of mechanical environment on the emergence of brass textures in FCC metals*, Acta Mater. 55 (3) (2007) 799–812, https://doi.org/10.1016/j.actamat.2006.07.017.

[49] Yazdani, M., Pot, C., Boyadjian, Q., Liu, Y., Yue, S., Béland, J.-F., and Bocher, P., *Effect of Unidirectional and Cross-Rolling on the Texture Evolution of a Hot Extruded AA6082*, in *Inalco 2023*. 2023. DOI: 10.3390/engproc2023043028.

[50] X.-F. Wang, M.-X. Guo, L.-Y. Cao, J.-R. Luo, J.-S. Zhang, L.-Z. Zhuang, *Influence of thermomechanical processing on microstructure, texture evolution and mechanical properties of Al–Mg–Si–Cu alloy sheets*, Trans. Nonferrous Met. Soc. Chin. 25 (6) (2015) 1752–1762, https://doi.org/10.1016/s1003-6326(15)63780-3.

[51] B. Bacroix, S. Queyreau, D. Chaubet, E. Siv, T. Chauveau, *The influence of the cube component on the mechanical behaviour of copper polycrystalline samples in tension*, Acta Mater. 160 (2018) 121–136, https://doi.org/10.1016/j.actamat.2018.08.044.
[52] F. Liu, Z. Liu, G. He, *Making Al-Cu-Mg alloy tough by Goss-oriented grain refinement*, J. Alloy. Compd. 904 (2022), https://doi.org/10.1016/j.jallcom.2022.164095.
[53] J. Hou, J. Qiao, J. Lian, P.K. Liaw, *Revealing the relationship between microstructures, textures, and mechanical behaviors of cold-rolled Al0.1CoCrFeNi high-entropy alloys*, Mater. Sci. Eng. A 804 (2021), https://doi.org/10.1016/j.msea.2021.140752.
[54] S.-K. Li, L.-X. Li, H. He, Z.-W. Liu, L. Zhang, *Influence of dynamic recrystallization on microstructure and mechanical properties of welding zone in Al–Mg–Si aluminum profile during porthole die extrusion*, Trans. Nonferrous Met. Soc. Chin. 29 (9) (2019) 1803–1815, https://doi.org/10.1016/s1003-6326(19)65088-0.
[55] C.N. Tomé, C.T. Necker, R.A. Lebensohn, *Mechanical anisotropy and grain interaction in recrystallized aluminum*, Metall. Mater. Trans. A 33 (8) (2002) 2635–2648, https://doi.org/10.1007/s11661-002-0385-x.
[56] V. Aryshenskii, F. Grechnikov, E. Aryshenskii, Y. Erisov, S. Konovalov, M. Tepterev, A. Kuzin, *Alloying elements effect on the Recrystallization Process in Magnesium-Rich Aluminum Alloy*, Materials (basel) 15 (20) (2022), https://doi.org/10.3390/ma15207062.
[57] Z. Ye, Z. Zhou, Z. Ye, Z. Wang, Q. Zhao, K.G. Prashanth, *An Investigation into the Thermomechanical Processing and Dynamic Recrystallization Mechanisms of High-Magnesium Aluminum Alloys*, Materials (basel) 18 (12) (2025), https://doi.org/10.3390/ma18122734.
[58] J. Gubicza, N.Q. Chinh, Z. Horita, T.G. Langdon, *Effect of Mg addition on microstructure and mechanical properties of aluminum*, Mater. Sci. Eng. A 387–389 (2004) 55–59, https://doi.org/10.1016/j.msea.2004.03.076.
[59] X. Qian, N. Parson, X.G. Chen, *Effects of Mn content on recrystallization resistance of AA6082 aluminum alloys during post-deformation annealing*, Journal of Materials Science & Technology 52 (2020) 189–197, https://doi.org/10.1016/j.jmst.2020.04.015.
[60] J. Rakhmonov, K. Liu, P. Rometsch, N. Parson, X.G. Chen, *Effects of Al(MnFe)Si dispersoids with different sizes and number densities on microstructure and ambient/elevated-temperature mechanical properties of extruded Al–Mg–Si AA6082 alloys with varying Mn content*, J. Alloy. Compd. 861 (2021), https://doi.org/10.1016/j.jallcom.2020.157937.
[61] Q. Zhao, K. Huang, Y. Li, K. Marthinsen, *Orientation Preference of Recrystallization in Supersaturated Aluminum Alloys Influenced by concurrent Precipitation*, Metall. Mater. Trans. A 47 (3) (2016) 1378–1388, https://doi.org/10.1007/s11661-015-3314-5.
[62] Y. Wu, H. Liao, J. Yang, K. Zhou, *Effect of Si Content on Dynamic Recrystallization of Al–Si–Mg Alloys during Hot Extrusion*, Journal of Materials Science & Technology 30 (12) (2014) 1271–1277, https://doi.org/10.1016/j.jmst.2014.07.011.